Nanoscale

Accepted Manuscript

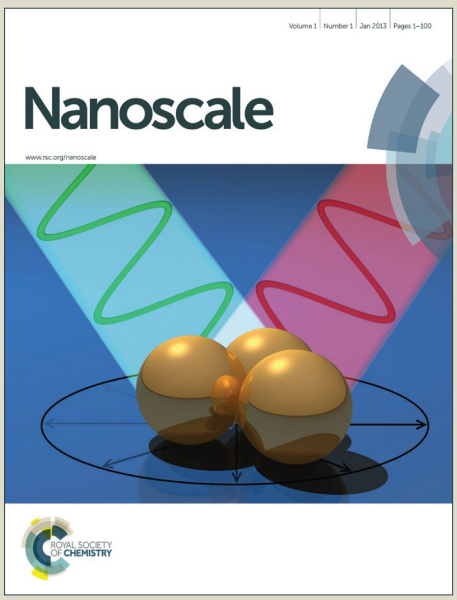

This is an *Accepted Manuscript*, which has been through the Royal Society of Chemistry peer review process and has been accepted for publication.

Accepted Manuscripts are published online shortly after acceptance, before technical editing, formatting and proof reading. Using this free service, authors can make their results available to the community, in citable form, before we publish the edited article. We will replace this *Accepted Manuscript* with the edited and formatted *Advance Article* as soon as it is available.

You can find more information about *Accepted Manuscripts* in the Information for Authors.

Please note that technical editing may introduce minor changes to the text and/or graphics, which may alter content. The journal's standard Terms & Conditions and the Ethical guidelines still apply. In no event shall the Royal Society of Chemistry be held responsible for any errors or omissions in this *Accepted Manuscript* or any consequences arising from the use of any information it contains.

ROYAL SOCIETY OF CHEMISTRY

www.rsc.org/nanoscale

Strong Interactions with Polyethylenimine-Coated Human Serum Albumin Nanoparticles (PEI-HSA NPs) Alter *α*- Synuclein Conformation and Aggregation Kinetics

Hossein Mohammad-Beigi[1,2,3], Seyed Abbas Shojaosadati [2], Amir Tayaranian Marvian [4], Jannik Nedergaard Pedersen [1], Lasse Hyldgaard Klausen [5], Gunna Christiansen [6], Jan Skov Pedersen [7], Mingdong Dong [5], Dina Morshedi [*3], Daniel E. Otzen[*1]

[1] Interdisciplinary Nanoscience Centre (iNANO) and Department of Molecular Biology and Genetics, Aarhus University, Gustav Wieds Vej 14, DK – 8000 Aarhus C

[2] Biotechnology Group, Faculty of Chemical Engineering, Tarbiat Modares University, P.O. Box 14115-143, Tehran, Iran

[3] Department of Industrial and Environmental Biotechnology, National Institute of Genetic Engineering and Biotechnology, P.O. Box: 1417863171, Tehran, Iran

[4] Department of Biomedicine, Aarhus University, 8000 Aarhus C, Denmark

[5] Interdisciplinary Nanoscience Centre (iNANO), Aarhus University, Gustav Wieds Vej 14, DK – 8000 Aarhus C

[6] Department of Biomedicine-Medical Microbiology and Immunology, Aarhus University, 8000 Aarhus C, Denmark

[7] Interdisciplinary Nanoscience Centre (iNANO) and Department of Chemistry, Aarhus University, Gustav Wieds Vej 14, DK – 8000 Aarhus C

Corresponding Authors: (D.E.Otzen) email: dao@inano.au.dk;(D.Morshedi) email: morshedi@nigeb.ac.ir;

Nanoscale Accepted Manuscript

Abstract

The interaction between nanoparticles (NPs) and the small intrinsically disordered protein *α*-synuclein (*α*SN), whose aggregation is central in the development of Parkinson's Disease, is of great relevance in biomedical applications of NPs as drug carriers. Here we showed using a combination of different techniques that *α*SN interacts strongly with positively charged polyethyleneimine-coated human serum albumin (PEI-HSA NPs), leading to a significant alteration in *α*SN secondary structure. In contrast, the weak interactions of *α*SN with HSA NPs allowed *α*SN to remain unfolded. These different levels of interactions had different effects on *α*SN aggregation. While the weakly interacting HSA NPs did not alter the aggregation kinetic parameters of *α*SN, the rate of primary nucleation increased in the presence of PEI-HSA NPs. The aggregation rate changed in a PEI-HSA NP-concentration dependent and size independent manner and led to fibrils which were covered with small aggregates. Furthermore, PEI-HSA NPs reduced the level of membrane-perturbing oligomers and reduced oligomer toxicity in cell assays, highlighting a potential role for NPs in reducing *α*SN pathogenicity *in vivo*. Collectivelly, our results highlight the fact that a simple modification of NPs can strongly modulate interactions with target proteins, which may have important and positive implications in NPs safety.

Keywords: Human Serum Albumin Nanoparticles, α- Synuclein, Polyethylenimine-Coated Human Serum Albumin Nanoparticles, Interaction, Conformation, Fibrillation.

Nanoscale Accepted Manuscript

1 Introduction

The 140 amino acid long-synuclein (αSN) protein is the main component of Parkinson's Disease (PD) associated deposits known as Lewy Bodies [1,2].αSN has three main region: an amphiphilic N-terminal part (residues 1-60) which initiates the interaction with membranes [3,4], a non-amyloid β-peptide component (NAC) region as the hydrophobic part of αSN which makes up the core of amyloid fibrils [4]; and an acidic C-terminus, which is unstructured in all forms of monomer and aggregates [4]. Although αSN, is known to be an intrinsically disordered protein [5], it is not completely unfolded and can assume conformations that are stabilized by long-range interactions between C terminus and the NAC regions, which inhibit oligomerization and aggregation [6,7]. αSN forms different forms of αSN oligomers and fibrils with various levels of interaction with membranes [8,9].

Different small molecules are known to inhibit the formation of toxic oligomers and fibrils [10–12].Because of the presence of the blood-brain barrier (BBB) as the homeostatic defense mechanism of the brain, various nanoparticles (NPs) have been designed to successfully transport small molecules specially hydrophilic ones across the BBB [13,14]. While several studies show that NPs with different structures interact with proteins and affect the fibrillation of proteins [15–19], there is limited data on the interaction of αSN with NPs and the effect on aggregation. For instance, acceleration of αSN fibrillation in the presence of αSN-conjugated CdSe/ZnS quantum dots was shown [20]. Yang *et al.*[21,22] also studied the interaction of αSN with negatively and positively charged gold NPs. αSN underwent multilayer adsorption on the surface of Au NPs via the N-terminus, based on strong electrostatic interactions in the hard corona and weaker non covalent protein-protein interaction in the soft corona [22]. No observable conformational change in αSN was induced by negatively charged NPs; however, αSN adopts a random orientation on positively charged Au NPs, with an increase in β- sheet and a decrease in α- helix structures [21]. On the other hand, αSN undergoes extensive conformational change when binding to negatively charged vesicles [23]. These reports suggest that in addition to electrostatics, interactions depend on the type of NPs which range from hard platform Au NPs to liquid ordered vesicles. Alvarez *et al.*[24] showed an accelerating

Nanoscale Accepted Manuscript

effect of negatively charged Au NPs with different sizes on the interaction of NPs; however, the change in the size of lipid vesicles had no effect on the fibrillation of αSN [25]. NPs also affect the toxicity of aggregates that form during fibrillation. For instance, dendrimers reduce toxicity of Aβ 1-28 peptide during aggregation along with accelerating formation of mature fibrils [26].

Human serum albumin (HSA) NPs are nontoxic, biodegradable, nonimmunogenic, and stable during storage [27] and are used to transport drugs across the BBB [14,28].Albumin protein with a negative charge at pH 7.4 is the main component of HSA NPs. Albumin is the most abundant protein in Cerebrospinal Fluid (CSF) and its concentration in CSF can increase from 3 up to 60 μM when the blood–CSF barrier is impaired [29]. Due to the presence of different binding sites and the high content of amine and carboxyl groups, HSA NPs can easily be coated with different ligands or polymers [30]. Polyethyleneimine (PEI), a cationic polymer, has been used to provide positive charges on the surface of HSA NPs to facilitate transport across the BBB and also to transport negatively charged small molecules [31].

Here we systematically assess (a) the nature of the interaction of HSA and PEI-coated HSA NPs (PEI-HSA NPs) with αSN, (b) the effect of the NPs on the kinetics of αSN aggregation, and (c) toxicity of aggregates that form in the presence of the NPs. We have applied a number of different techniques to assess this. Centrifugation methods, small angle X-ray scattering (SAXS), circular dichroism (CD) and fluorescence anisotropy confirmed the stronger interaction of αSN with PEI-HSA NPs and the change in the secondary structure of αSN. Thioflavin T fluorescence time profiles reveal that PEI-HSA NPs promote the primary nucleation step without changing the growth rate and secondary pathway. Atomic force microscopy (AFM) indicated formation of small globular aggregates in the plateau region of samples with PEI-HSA NPs. Finally, a cellular toxicity assay showed that the aggregates formed in the presence of the NPs are less toxic than those formed without the NPs.

Nanoscale Accepted Manuscript

2 Materials and methods

2.1 Preparation of HSA NPs

HSA NPs with four different sizes were prepared based on a desolvation technique using methanol, ethanol, acetone or acetonitrile as the solvent as described previously [31]. Briefly, 100 mg of HSA was dissolved in 1.0 mL of 10 mM NaCl solution and the pH was adjusted to 8.2. Particle formation was performed by drop-wise addition of the solvent to HSA solution at the rate of 1.0 mL/min under continuous stirring (550 rpm) until the solution became turbid. Subsequently, 60 μL of 8% glutaraldehyde solution was added to induce particle crosslinking by stirring for 12 h. The resulting NPs were purified by three cycles of centrifugation (28,000×g, 25 min at 4°C) and redispersion of the pellets to the original volume in 10 mM NaCl.

2.2 Preparation of PEI-HSA NPs

Details of the PEI coating HSA NPs method have been published previously [31] and only a brief summary is given here. PEI-HSA NPs were prepared through coating HSA NPs with PEI via covalent amide bond formation between the amine groups of PEI and carboxyl groups of HSA NPs using N-hydroxysuccinimide (NHS), N-(3-dimethylaminopropyl)-N-ethylcarbodiimide hydrochloride (EDC.HCl). 1 mL phosphate-buffered saline (PBS) buffer (10 mM, pH 7.4) containing NHS (0.2 mg/mL), EDC (1 mg/mL), and sonicated HSA NPs (5 mg/mL) was stirred slowly for 7 min. The particles were collected by centrifugation and the resulting carboxyl activated NPs were resuspended to 2 mL PBS buffer containing PEI (5 mg/mL). The coating was allowed to proceed for 1 h and the NPs were collected by centrifugation and washed three times with PBS buffer, and finally redispersed in deionized-water.

2.3 Protein handling

αSN was expressed in *Escherichia coli* BL21(DE3) and purified as described in Lorenzen *et al.*[32] and Supplementary Information (SI). Prior to use, freshly dissolved αSN in PBS buffer (20 mM phosphate, 150 mM NaCl, pH 7.4) was filtered (0.2 μm). Protein concentration was measured by absorbance measurements at 280

Nanoscale Accepted Manuscript

nm with a NanoDrop™ 1000 spectrophotometer (Thermo Scientific) using a theoretical extinction coefficient of 0.412 $(mg/mL)^{-1}$.

2.4 Circular dichroism(CD) spectroscopy

For far-UV CD, sonicated fibril solutions with protein concentration of 0.2 mg/mL (14 μM) were put in a 1 mm cuvette and the spectra were measured from 250 to 195 nm at 25 °C with a Jasco J-810 spectrophotometer (Jasco Spectroscopic Co. Ltd., Japan). To measure the induced changes in the secondary structure of αSN by NPs, 0.2 mg/mL of αSN was mixed with 0.1 mg/mL of HSA NPs and different concentrations of PEI-HSA NPs (25-100 μg/mL) in PBS buffer. CD spectra of PBS buffer and the NPs were recorded and subtracted from the protein spectra and the CD signal given as mean residue ellipticity (degrees cm^2 $dmol^{-1}$).

2.5 Adsorption of αSN onto the surface of NPs

Centrifugation was used to separate free proteins from a denser particle/protein complex. Solutions of the NPs in PBS buffer at 0.5 mg/mL concentration with different αSN concentrations (0.2, 0.3, 0.5, 1, and 2 mg/ml) were incubated for 30 min at 37 °C. The solutions were then centrifuged (14500, 20 min) and the absorbance of free protein was measured at 280 nm with a NanoDrop™ 1000 spectrophotometer (Thermo Scientific). The Langmuir equation was used to determine the binding constant of αSN to HSA and PEI-HSA NPs.

$$q_e = \frac{q_m K_L C_e}{1 + K_L C_e} \qquad (3)$$

where q_e is the equilibrium adsorption capacity (mg/g), C_e is the equilibrium liquid phase concentration, (mg/L), q_m is the adsorption capacity, (mg/g), and K_L is adsorption equilibrium constant, (L/mg).

2.6 Fluorescence labeling of αSN monomers

Labeling was carried out by using asuccinimidyl ester of Fluor 594 carboxylic acid (Invitrogen) according to the manufacturer's instructions, leading to a labeling molar ratio of 0.5 (dye to protein).

2.7 Fluorescence anisotropy

Nanoscale Accepted Manuscript

Fluorescence anisotropy was used to measure changes in rotational correlation time of the molecule. The binding of αSN to the NPs is therefore expected to change the anisotropy. Fluorescence anisotropy was measured by a LS 55 Luminescence Spectrometer (Perkin Elmer). Samples were excited with vertically polarized light at 594 nm, and the emission intensity was measured at 617 nm through both parallel and perpendicular polarizers. The anisotropies were obtained at a protein concentration of 2 μM and a NPs concentration of 0.5 mg/mL.

2.8 Small-angle X-ray scattering (SAXS)

Samples for SAXS were prepared by incubating 0.5 mg/mL NPs in PBS buffer with 1 mg/mL αSN for 30 min at 37 °C. Solutions containing only NPs or only αSN at the above concentrations were used as control samples. Samples were measured on a flux and background optimized NanoSTAR SAXS camera from Bruker AXS located at Aarhus University [33]. Due to the relatively large size of the NPs, the camera was set up for measuring at low angle using a first pinhole after the optics of 0.75 mm Ø and a square hombuilt 'scatterless' slit [34] (0.5 × 0.5 mm^2), a sample-detector distance of 107 cm and a pinhole of 2.0 mm Ø. The acquisition time was 60 min for all samples and background buffers and conversion to absolute scale was done with the SUPERSAXS program package (C.L.P. Oliveira and J.S. Pedersen, unpublished). The intensity is presented as a function of the magnitude of the scattering vector $q = 4\pi\sin\theta/\lambda$, where λ=1.54 Å is the wavelength and 2θ is the scattering angle.

The pair distance distribution function $p(r)$ was calculated using the indirect Fourier transformation (IFT) method [35] implemented in the WIFT program [36]. The function $p(r)$ is a histogram over distances between pairs of points within the particle, weighted by the excess scattering length density at the points. It thus gives information about the particle size and shape in real space.

A model of polydisperse spheres, consistent with the p(r) functions, was also fitted to the data. The number size distribution was described by a Gaussian and a Lorentzian term with a scale factor was added to the scattering

Nanoscale Accepted Manuscript

from the polydisperse spheres for describing random parts of the αSN or free αSN. The expressions for scattering model can be found in [37].

2.9 Plate reader fibril formation assays

αSN fibril formationwas carried out as previously described [38]. Briefly, 150 μL PBS solution containing70 μM αSN, 40 μM ThT and increasing concentration of NPs was added to each well of a 96-well-plate (Nunc, Thermo Fischer Scientific, Roskilde, Denmark) with a 3 mm diameter glass bead. Plates were sealed with Crystal clear sealing tape (Hampton Research, Aliso Viejo, CA). The fibrillation was followed at a Genios Pro fluorescence plate reader (Tecan, Männerdorf, Switzerland) at 37 °C with 300 rpm orbital shaking between the readings for 12 min. Samples were excited at 448 nm and emission was measured at 485 nm. To study the effect of salt concentration, the NPs were added to αSN solutions with different salt concentrations (50 – 300 mM NaCl). The Finke-Watzky (F-W) two step model [39] was fitted to the normalized ThT fibrillation data:

$$F(t) = \frac{1}{1+e^{-4v(t-t_{1/2})}} \qquad (1)$$

$$t_N = t_{1/2} - \frac{1}{2v} \qquad (2)$$

where $t_{1/2}$ is the time required to produce half the total product, v is the rate of growth at that time, and t_N is the duration of the nucleation phase.

2.10 Oligomerization assays

1 mg/mL αSN monomer was incubated on an Eppendorf thermoshaker, TS-100, BioSan, Latvia with 50 μg/mL of NPs for 1 h at 37 °C and 900 rpm. The solution was centrifuged (14500 rpm, 20 min) and the supernatant was injected into a 24 mL superpose 6 10/300 column, GE Healthcare Lifescience for separating different αSN species.

2.11 Preparation of Large Unilamellar Vesicles (LUVs)

Nanoscale Accepted Manuscript

LUVs were prepared as described before [40]. Briefly, 1, 2-dioleoyl-sn-3-phosphatidylglycerol (DOPG) wasdissolved at 5 mg/ml in PBS in the presence of calcein at self- quenching concentration (70 mM). The solution was subjected to 10 freeze thaw cycles between liquid nitrogen and a 50 °C water bath. The lipid solution was extruded 21 times through a 100 nm filter. After extrusion, vesicles solution wasrun on a PD-10 desalting column (GE Healthcare) to separate the free calcein from calcein entrapped vesicles.

2.12 Calcein release assays

Permeabilization of vesicles due to the interaction with oligomers results in calcein release and an increase in the fluorescence signal due to the dilution. DOPG vesicles at a final lipid concentration of 42 μM were loaded in triplicate in a 140 μL assay solution onto a 96-well plate (Nunc, Thermo Fisher Scientific, Roskilde, Denmark). The lipid concentration is based on an estimated two-fold dilution of the vesicles in the desalting step. The background fluorescence at excitation 485 nm and emission at 520 nm was measured on Genios Pro fluorescence plate reader (Tecan, Mänerdorf, Switzerland) before and after addition of vesicles. The NPs and/ or oligomers at a final concentration of 1-100 μg/mL and 0.5 μM, respectively,were mixed with vesicles in a final volume of 150 μL. The plates were sealed with crystal clear sealing tape (Hampton Research, Aliso Viejo, CA) and calcein release was measured for 1 h at 37 °C and a 2-s autoshake. Finally, 1 μL Triton X-100 (0.1% (w/V)) was added to measure the saturated end-level of fluorescence. Background fluorescence was subtracted.

2.13 Evaluation of cell viability

The 3-[4, 5-dimethylthiazol-2-yl]-2,5-diphenyltetrazolium bromide (MTT) assay was implemented to measure cellular viability after 24 h treatment by monomeric or aggregated forms of αSN. PC-12 Cells were seeded in 96 well-plates at the concentration of 30000 cells/100 μL/well in Dulbecco's Modified Eagle Medium (DMEM) supplemented with 10 % fetal bovine serum (FBS), 100 units/mL penicillin, and100 μg/mL streptomycin and cultured for 24 h. Media were then replaced with fresh media containing 7.5 % αSN samples (collected during the fibrillation process). After 24 hours treatment, the old media were replaced with fresh ones containing 10 %

Nanoscale Accepted Manuscript

MTT (5 mg/mL), and the plates were incubated for an additional 4 h at 37 °C. The MTT solution was removed and replaced by 100 μL DMSO in order to dissolve Formazan crystals through incubating 1 hour on shaking table at room temperature. Ultimately, absorbance was determined by a plate reader at 570 nm using 650 nm as a reference wavelength.

Note: Details of protein production and purification, fibril elongation assays, fibril disaggregation assays, preparation of oligomers, and structural and morphology characterization of fibrils by transmission electron microscopy (TEM), atomic force microscopy (AFM), and attenuated total reflectance Fourier transform infrared spectroscopy (ATR-FTIR) are provided in SI.

Nanoscale Accepted Manuscript

3 Results and discussion

3.1 Centrifugation, Fluorescence Anisotropy, Small-Angle X-ray Scattering (SAXS), and Circular Dichroism (CD) Confirm the Strong Interaction of *α*SN and PEI-HSA NPs

HSA NPs were synthesized using the desolvation method, leading to an average zeta potential of -36±3.1 mV. When the cationic polymer PEI was used to coat the surface of HSA NPs, the zeta potential value of the NPs increased to +35 ± 2.8 mV. The NPs were imaged by TEM (Fig. S1). The TEM images confirmed the spherical shape of HSA and PEI-HSA NPs.

To explore the nature of the interaction of *α*SN with HSA and PEI-HSA NPs, centrifugation, fluorescence anisotropy, small-angle X-ray scattering (SAXS), and circular dichroism (CD) were used. 0.2-2 mg/ml *α*SN was incubated for 0.5 h with 0.5 mg/mL NPs. Subsequently we used centrifugation to pellet particle-protein complexes and separate free and weakly bound *α*SN from strongly attached *α*SN. Most of the *α*SN incubated with HSA NPs remains unbound in the solution after centrifugation (Fig. 1A), which shows that substantial proportion of the *α*SN either do not bind to HSA NPs, or bind reversibly and exchange with proteins in the bulk during centrifugation, aided by shear forces [41]. In contrast, *α*SN shows strong binding to PEI-HSA NPs, which may be caused by electrostatic interactions between PEI and *α*SN. The Langmuir equation was used to determine the binding constant of *α*SN to HSA and PEI-HSA NPs. This model could fit binding of *α*SN to PEI-HSA NPs, giving an equilibrium adsorption capacity (q_{max}) of 1.24±0.11 mg/mg and an adsorption equilibrium constant (K_L) of 0.598 ± 0.08 L/g (regression coefficient (R^2) = 0.989) . This model could also fit binding of *α*SN to HSA NPs but with lower confidence (R^2 = 0.92), giving a q_{max} of 0.71±0.27 mg/mg and K_L of 0.23±0.13 L/g. The Langmuir model is based on the fact that on the surface of NPs, a monomolecular layer of protein is formed, and all active sites are identical and energetically equivalent [31]. So, the reduced confidence of the fit for the model

Nanoscale Accepted Manuscript

for adsorption of αSN on HSA NPs can be due to the combined results of a too weak interaction between αSN and HSA NPs and inhomogeneous active sites on the surface of HSA NPs for αSN.

Fluorescence anisotropy was used to measure changes in rotational correlation time of the αSN. If the rotational Brownian motion of αSN is slowed down by the attachment of fluorophores to the NPs, the anisotropy will be increased [42]. Indeed, we saw a significant increase in the fluorescence anisotropy of αSN when added to PEI-HSA NPs but not to HSA NPs (Fig. 1B), which confirms the observation from centrifugation experiments that αSN binds strongly to PEI-HSA NPs but not to HSA NPs.

We turned to SAXS to elucidate whether NP-αSN interactions would lead to significant changes in shape or size of the two components (Fig. 1C). αSN as an intrinsically disordered protein has a radius of gyration (R_g) of 40 Å. This value is less than the R_g of a completely random-coil chain (52 Å) but much greater than that of a globular protein of 140 residues (15.1 Å), showing that αSN is unfolded but more compact than a completely unfolded and random coil [43]. We have earlier shown that small amounts of αSN oligomers are present in freshly dissolved αSN solutions, giving a higher scattering intensity $I(q)$ at low q than would be expected from αSN monomer [44]. However, the NPs have a much larger mass than αSN, so that free αSN hardly contributes to total scattering at low q when the NPs and αSN are mixed.

Indirect Fourier transformation of data was used to obtain a pair distance distribution function $p(r)$ (Fig. S2), which provides information on the structure of the particles. The shape of the $p(r)$ function suggested a nearly spherical shape for the NPs both with and without αSN monomer. The NPs have some degree of polydispersity and therefore a model with spherical particles with polydispersity was used to fit the SAXS data and describe the αSN-NP complex.

The first fits showed that the polydispersity of the particles and complexes is very similar and close to 18%. The polydispersity was then fixed to 18 % and only the average size was varied.The size of the particles and the scale

Nanoscale Accepted Manuscript

of fluctuation term are given in Table 1. The radius of PEI-HSA NPs (37.3±0.2 nm) was slightly larger than that of HSA NPs (36.2±0.3 nm) due to the polyethylenimine layer on the PEI-HSA NPs. As the random parts outside the particle will contribute only to the hydrodynamics of the particle, the size obtained by SAXS is expected to be slightly smaller than the hydrodynamic radius determined by DLS [37] (41 nm and 37.5 nm for PEI-HSA NPs and HSA NPs, respectively). Upon addition of αSN to the HSA NPs, no significant change in the size of HSA NPs could be seen (36.0±0.2 nm) showing that αSN do not tightly interact with the NPs. However, addition of αSN to the PEI-HSA NPs increased the size of the particles (39.2±0.3 nm) demonstrating that a layer of αSN had attached to the particle surface. To obtain a proper fit with the model, a fluctuation term taken as a Lorenzian function with a scale and a correlation length of 30 Å (fixed) was included that takes into account the signal from free αSN monomer and loosely bound αSN on the NP surface. For PEI-HSA NPs,the scale of the term is higher (27±9 in arbitrary units) than HSA NPs (1.3±1.2) which could be due to PEI being bound in a flexible conformation on the surface of the NPs. When αSN is added to the NPs, an increase in the scale for both HSA NPs (152±11) and PEI-HSA NPs (132±9) is seen. The smaller value for PEI-HSA NPs compared to HSA NPs could be due to smaller amounts of free αSN in solution, since αSN is bound to the NP surface.

Taken together, evidence from several different analytical approaches shows that the interaction between PEI-HSA NPs and αSN is stronger than the interaction between αSN and HSA NPs. This evidence can be summarized as follows: Firstly, 1.75 more αSN remains bound to the surface of PEI-HSA NPs after centrifugation. Secondly, the fluorescence anisotropy of αSN increases 9 times more when added to PEI-HSA NPs than to HSA NPs. Thirdly, PEI-HSA NPs increases more in size than HSA NPs upon addition of αSN.

To explore whether the structure of αSN changes after mixing with the NPs, far-UV circular dichroism spectroscopy (CD) was used. The mass ratio of αSN to HSA NPs was maintained at 2:1. αSN adsorption onto HSA NPs did not induce any observable spectral change, *i.e.* αSN keeps its unstructured nature when adsorbed (Fig.1D). In contrast, addition of different concentrations of PEI-HSA NPs (20 – 200 μg/mL) caused a

Nanoscale Accepted Manuscript

significant change in the secondary conformation of αSN (Fig.1E), which can lead to exposure of the hydrophobic NAC region to the solvent and increasing the number of nucleation events [7]. PEI by itself does not cause significant change in αSN's secondary structure (Fig. 1F) [45]. The lack of conformational change in the presence of PEI polymer and HSA NPs and the change of secondary conformation in αSN due to interaction with PEI-HSA NPs confirm that PEI-HSA NPs interact more strongly with αSN than PEI polymer and HSA NPs.

Combining the data obtained from the different analytical approaches, we conclude that interaction of αSN and PEI-HSA NPs is strong and leads to conformational change in αSN.

3.2 The Presence of PEI-HSA NPs Alters the Aggregation Kinetics of αSN

To explore the effect of HSA and PEI-HSA NPs on αSN aggregation via week and strong interactions, respectively, ThT assay was used to systemically study the kinetic of aggregation of αSN after mixing with the NPs.

5-100 μg/mL of negatively charged HSA NPs (hydrodynamic diameter = 75 nm) had no significant effect on the kinetics of fibrillation of αSN (Fig.2A), which contrasts with other negatively charged NPs. For instance, various concentrations of negatively charged gold NPs of different sizes (10-22 nm) strongly accelerate αSN aggregation, increasing both the nucleation and growth rate of the overall mechanism [24]. Furthermore, binding of αSN to anionic lipid vesicles (20-100 nm) can enhance the rate of primary nucleation by three orders of magnitude (20-100 nm) [25]. The anionic polymer heparin also accelerates αSN fibrillation due to the presence of specific heparin-binding sites in the N-terminal region of αSN [46].

In the next step, we studied the effect of PEI- HSA NPs (82 nm) on the kinetics of αSN fibrillation. αSN fibrillation is dramatically accelerated in the presence of PEI [45]. ThT data showed that PEI-HSA NPs also accelerate the fibrillation of αSN in a dose dependent manner; however, ThT data reach the same plateau value

Nanoscale Accepted Manuscript

either in the presence or absence of PEI-HSA NPs (Fig.2B). Increasing the PEI-HSA NPs concentration above 100 μg/mL does not further affect aggregation kinetics (data not shown). These results are contrary to those of Taebnia*et al.*[47] who showed that αSN fibril formation is reduced considerably in the presence of PEI-coated mesoporous silica nanoparticles (PEI-MSNPs).

To quantify the effect of the NPs on the fibrillation kinetics, the Finke-Watzky model was fitted to the ThT data (Fig.2 C-E). PEI-HSA NPs produced a concentration dependent reduction of the lag phase and half time; the highest concentrations produced the strongest reduction in the lag phase and half time; however, PEI-HSA NPs had no effect on the growth rate of αSN at different concentrations. Polycations mainly interact with C-terminal residues of αSN [7]. These interactions can decrease the repulsion of neighboring αSN molecules and increase the local concentration of αSN on the surface of PEI-HSA NPs [48]. Although the relative lag and half time parameters decreased by increasing the PEI-HSA NPs, the growth rate did not changed compared to the control.

Fig.S3 shows that the kinetic parameters of αSN are not dependent on the sizes of either HSA (75, 100, 155, and 280 nm) or PEI-HSA NPs (82 and 180 nm), at least in the ranges that were used in our study. Galvagnion *et al.*[25] also showed that membrane curvature of vesicles of >20 nm and <100 nm does not have a major role for either the binding or nucleation of αSN. However, Alvarez *et al.* [24] showed that the smaller Au NPs with curvature comparable to αSN (10 nm) lead to the greatest effect on the acceleration of the aggregation.

3.3 HSA and PEI-HSA NPs Do Not Change the Secondary Pathway of αSN Aggregation

To determine whether or not the NPs can affect the secondary pathway (secondary nucleation and/ or fragmentation) of αSN aggregation, seeding was used to bypass the primary nucleation and study the secondary nucleation as the main pathway responsible for the proliferation of fibrils [48]. Secondary nucleation (surface catalysed nucleation building on existing aggregates) creates aggregates at a rate that will depend on the concentration of both monomeric αSN and existing aggregates. Here we added short fibrillar seeds (5 %) to

Nanoscale Accepted Manuscript

monomeric αSN (1 mg/mL) to accelerate the nucleation phase of amyloid formation via seeding under shaking. Then the NPs (50 μg/mL) were added to monomeric αSN containing seeds. As shown above, PEI-HSA NPs accelerated the fibrillation of αSN in the experiments without seeds (Fig.2B) and therefore must promote nucleation events leading to fibrils. However, they did not affect the lag phase in the presence of seeds (Fig. S4A). We therefore conclude that the NPs do not affect secondary nucleation. Rather, they likely promote heterogeneous primary nucleation by providing a surface on which the monomers can nucleate and start the fibrillation process. After formation of such a primary nucleus on the surface of PEI-HSA NPs, the elongation continues with the same growth rate compared to the samples without the NPs and the secondary nucleation occurs on the surface of the growing aggregates without any additional participation by NPs.

We also added 50 μg/mL HSA and PEI-HSA NPs to the final mixture of αSN monomers and aggregates to assess whether or not the NPs can reverse fibrillation or change the final chemical equilibrium and start a new aggregation. ThT signals showed no effect of the NPs on the premade fibrils (Fig.S4 B) , and TEM images also indicated no significant difference in the structure of fibrils (data not shown).

These findings suggest that PEI-HSA NPs induce a catalytic mechanism in the primary nucleation step without changing the growth rate and secondary pathway (secondary nucleation and fragmentation). The seeding assay also confirms that when there are enough preformed seeds to start elongation, PEI-HSA NPs do not affect the growth rate. On the other hand, PEI-HSA NPs could not dissociate the preformed fibrils. Unlike primary and secondary nucleation that are dependent on free monomers and do not affect kinetics at late stages in the reaction, fragmentation and dissociation play significant roles in the establishment of chemical equilibrium between monomeric and fibrillary protein [49]. The end point signals of ThT without and with PEI-HSA NPs are almost the same. This means that the NPs do not change the extent of fibrillation, which in turn means they do not change the equilibrium between monomer and fibril. Furthermore, they have no effect on the dissociation and fragmentation rate. Rather, the effect of PEI-HSA NPs during αSN fibril formation is to accelerate

Nanoscale Accepted Manuscript

nucleation. We provide a scheme (Fig. 3) which shows the possible mechanism of the effect of HSA and PEI-HSA NPs on *α*SN's adsorption, orientation and aggregation based on the experimental data obtained in this work.

3.4 Factors besides Electrostatic Interactions Can Affect the Primary Nucleation of *α*SN on PEI-HSA NPs

To further understand the mechanism of the effect of HSA and PEI-HSA NPs on αSN fibrillation, the effect of the NPs on *α*SN aggregation at different NaCl concentrations (50-300 mM) was studied. The ThT data and associated kinetic parameters (Fig.4) indicate that increasing NaCl concentration induces an increase in the extent of fibrillation (was confirmed by ThT data and TEM images (Fig.S5)), which could be due to the change in the availability of water molecules, thus changing the thermodynamic properties of the fibrils such as solution activity of *α*SN [50]. Furthermore, an increase in NaCl concentration led to a significant decrease in $t_{½}$ and t_{nuc}, but only a slight increase in growth rate. Like at 150 mM NaCl concentration, HSA NPs did not show significant effect on the kinetic parameters and endpoint ThT fluorescence at other NaCl concentrations, which shows that changing the NaCl concentration cannot affect the interaction of *α*SN and HSA NPs. The parameters $t_{½}$ and t_{nuc} did not change in the presence of PEI-HSA NPs at different NaCl concentrations; however, the growth rate slightly changed. In contrast, Galvagnion *et al.*[25] showed that the NaCl concentration can influence the interaction of *α*SN and vesicles. However, since increasing NaCl concentration did not have an effect on the primary interaction of PEI-HSA NPs and *α*SN, we believe that factors besides electrostatic interactionscan affect the primary nucleation of *α*SN on PEI-HSA NPs.

Combining the data obtained from the different techniques in this work and other studies [21,25,51],we conclude that the interactions depend on the charges of NPs, and whether or not the interaction is dependent on the size of NPs is dependent on the nature of the particle surface. For instance, the interaction is dependent on the both charges

Nanoscale Accepted Manuscript

and sizes of Au NPs [21] , but it is independent of vesicle sizes (in the range of 20-100 nm) [25], HSA NPs (in the range of 75-280 nm) and PEI-HSA NPs (in the range of 82-180 nm).

3.5 The NPs Do Not Affect the Structure of *α*SN Fibrils, while Small Spherical Aggregates Form in the Presence of PEI-HSA NPs

Structural analysis of *α*SN fibrils formed alone or in the presence of either HSA NPs or PEI-HSA NPs has been made using CD and ATR-FTIR (Fig. S6). The CD spectra of the monomers resembles the classical spectrum of an unstructured protein andthe *β*-sheet structures of fibrils are characterized with a negative peak at 222 nm and a positive at 204 nm. ATR-FTIR spectra of *α*SN fibrils and their deconvolution shows maximum at 1629 , 1654, and 1673 cm^{-1} indicative of antiparallel *β*-sheet structure, unordered structures, and turn or *β*-sheet, respectively [52]. Deconvolution of the spectra showsthat there is no significant difference between *β*-sheet and unordered content of *α*SN fibrils formed alone compared with those formed in the presence of HSA and PEI-HSA NPs (Table 2).

The effect of the NPs on the morphology of *α*SN aggregates formed at different time courses (1 and 4 h) during the fibrillation process was analyzed using TEM (Fig.5A). TEM images of both *α*SN incubated alone or in the presence of HSA NPs showed small crowded oligomers after 1 h and larger aggregates after 4 h, while *α*SN fibrils gradually appeared in the presence of PEI-HSA starting from 1 h.

The morphology of the fibrils in the plateau region of ThT fluorescence were studied by TEM and AFM (Fig.5). Both TEM and AFM images showed coexistence of ribbon and helical ribbon-like fibril structures. Zhang *et al.*[53] showed that flat ribbons twist into helical fibrils, which are smother. As this process is very slow, both structure can coexist at the end of fibrillation. TEM images showed that there are no significant differences between fibrils formed at different salt concentration in the presence or absence of HSA NPs and PEI-HSA NPs (Fig. S5).

Nanoscale Accepted Manuscript

However, more fibrils were observed at higher salt concentration, leading at 300 mM to long fibrils that were tightly stacked on top of each other.

Based on AFM analysis, the average periodicity of the twisted fibrils in all samples with and without the NPs were about 200 nm and most were in the range 150- 250 nm (Fig.5D). In the samples with PEI-HSA NPs, three distinct types of structures were present. Fibrils with a height of around 8 nm covered by small spherical species with a height of about 20 nm (Fig.5F, less than the height of PEI-HSA NPs, 70 nm (Fig.5G)), and other spherical species with a height of about 70 nm that can be attributed to large aggregates and/or PEI-HSA NPs that acted as seeds to start nucleation.

3.6 PEI-HSA NPs Reduce the Level of Membrane-Perturbing Oligomers

In order to study the effect of the NPs on soluble aggregates, we prepared oligomeric species of αSN using our previously developed method [54], removing insoluble species by centrifugation and separating the supernatant on a gel filtration column. This allows us to focus on the formation of soluble species larger than monomeric αSN.

Under these conditions, αSN forms two populations of oligomers after 1 h which correspond to elongated large and small spherical oligomers [54]. SEC analysis revealed that the amounts of small oligomers in the presence of HSA NPs had no significant difference with control (Fig.6). However, PEI-HSA NPs dramatically decreased the amount of small oligomer to a level comparable to that of the large oligomers.

3.7 PEI-HSA NPs Reduce the Perturbation of Oligomers in Membranes

As a first step to investigate potential toxicity of αSN aggregates formed at different time courses, calcein release assay was used to investigate if the NPs can decrease or increase the membrane permeabilization by αSN oligomers (0.5 μM). The NPs alone did not lead to any calcein release up to 10 μg/ml; above this concentration range, PEI-HSA NPs alone led to significant release while HSA NPs had no effect (Fig.7 A and B). This is

Nanoscale Accepted Manuscript

consistent with the observation that PEI-HSA NPs at higher concentrations (>100 μg/mL) show a slight increase in free radical formation in PC-12 cells [31]. Consequently, we only investigated NPs concentrations up to 10 μg/ml. PEI-HSA NPs can decrease calcein release in a dose response fashion (from 65 % to 37 %), while HSA NPs showed a weaker inhibitory effect (from 65 % to 52 %, respectively).

3.8 Toxicity of Formed Aggregates Decreases in the Presence of the NPs

To evaluate the toxicity of formed aggregates during the fibrillation process, samples were taken at different time courses (0, 0.5, 1.5, 4, 8, 10, 12, and 24 h). The toxicity of the aggregates was assessed on PC-12 cells using MTT. Neuroendocrine PC-12 cells have the capability to produce the neurotransmitter dopamine (DA) and contain functional DA metabolism pathways. In the control experiments the toxic effects of the aggregates progressed for up to 10 h and then decreased (Fig.8); however, the final aggregates were still toxic which could be due to the toxicity of the mature fibrils and/or the presence of off-pathway oligomers that cannot elongate to fibrilsand coexist with mature fibrils [9]. Cell toxicity of aggregates formed in the presence of NPs shows a similarity in trends with controls ones, but differences in cell viability and the times for minimal cell viability. Aggregates that formed in the presence of PEI-HSA NPs at two different concentrations (25 and 50 μg/mL) were less toxic than those formed in the presence of HSA NPs and profoundly less than the control ones.

The reduced toxicity of the formed aggregates in the presence of PEI-HSA NPs may arise from a number of figures. Incubation of αSN in the presence of PEI-HSA NPs reduced the level of off-pathway oligomers. On the other hand, the calcein release assay showed that PEI-HSA NPs can slightly decrease the interaction of oligomers and vesicles.

4 Conclusion

We report here that it is possible to modulate the interaction of αSN and NPs by modifying the surface of NPs, which can have critical implication in NPs safety. Using a combination of experimental approaches, we showed

Nanoscale Accepted Manuscript

that while the weak interaction between *α*SN and negatively charged HSA NPs cannot alter conformation and kinetics of aggregation of *α*SN, there is a strong interaction between *α*SN and PEI-HSA NPs that alters the *α*SN secondary structure and accelerates the primary nucleation of *α*SN fibrillation. Comparing our results with previous works, we conclude that other than the charge of NPs, the chemical composition of NPs can affect their interaction with *α*SN.

PEI-HSA NPs reduced the formation of oligomers, level of membrane-perturbing oligomers and oligomer toxicity in cell assays. Thus, in contrast to the view that the toxicity is best reduced by stopping the fibrillation, we provide evidence that acceleration of the formation of mature fibrils which have less toxicity can be a useful therapeutic approach. These finding show that both HSA NPs and PEI-HSA NPs that have no effect and accelerate the fibrillation *α*SN, respectively, can be used as drug carriers to transport drugs across the BBB. The potential of the NPs to be used as drug carriers and the effect of drugloaded NPs on the kinetics of aggregation of *α*SN and the level of toxicity of formed aggregates are under study.

REFERENCES

1. M. G. Spillantini, M. L. Schmidt, V. M.-Y. Lee, J. Q. Trojanowski, R. Jakes, and M. Goedert, *Nature*, 1997, **388**, 839–840.

2. B. Winner, R. Jappelli, S. K. Maji, P. A. Desplats, L. Boyer, S. Aigner, C. Hetzer, T. Loher, M. Vilar, S. Campioni, and others, *Proceedings of the National Academy of Sciences*, 2011, 201100976.

3. A. S. Maltsev, J. Chen, R. L. Levine, and A. Bax, *Journal of the American Chemical Society*, 2013, **135**, 2943–2946.

4. B. Van Rooijen, K. van Leijenhorst-Groener, M. Claessens, and V. Subramaniam, *Journal of molecular biology*, 2009, **394**, 826–833.

5. B. Fauvet, M. K. Mbefo, M.-B. Fares, C. Desobry, S. Michael, M. T. Ardah, E. Tsika, P. Coune, M. Prudent, N. Lion, and others, *Journal of Biological Chemistry*, 2012, **287**, 15345–15364.

Nanoscale Accepted Manuscript

6. C. W. Bertoncini, Y.-S. Jung, C. O. Fernandez, W. Hoyer, C. Griesinger, T. M. Jovin, and M. Zweckstetter, *Proceedings of the National Academy of Sciences of the United States of America*, 2005, **102**, 1430–1435.

7. C. O. Fernández, W. Hoyer, M. Zweckstetter, E. A. Jares-Erijman, V. Subramaniam, C. Griesinger, and T. M. Jovin, *The EMBO journal*, 2004, **23**, 2039–2046.

8. L. Bousset, L. Pieri, G. Ruiz-Arlandis, J. Gath, P. H. Jensen, B. Habenstein, K. Madiona, V. Olieric, A. Böckmann, B. H. Meier, and others, *Nature communications*, 2013, **4**.

9. W. Paslawski, S. Mysling, K. Thomsen, T. J. Jørgensen, and D. E. Otzen, *Angewandte Chemie International Edition*, 2014, **53**, 7560–7563.

10. N. Lorenzen, S. B. Nielsen, Y. Yoshimura, B. S. Vad, C. B. Andersen, C. Betzer, J. D. Kaspersen, G. Christiansen, J. S. Pedersen, P. H. Jensen, and others, *Journal of Biological Chemistry*, 2014, **289**, 21299–21310.

11. M. T. Ardah, K. E. Paleologou, G. Lv, S. B. A. Khair, A. S. Kazim, S. T. Minhas, T. H. Al-Tel, A. A. Al-Hayani, M. E. Haque, D. Eliezer, and others, *Frontiers in aging neuroscience*, 2014, **6**.

12. Y. Liu, J. A. Carver, A. N. Calabrese, and T. L. Pukala, *Biochimica et Biophysica Acta (BBA)-Proteins and Proteomics*, 2014.

13. T. Kanazawa, F. Akiyama, S. Kakizaki, Y. Takashima, and Y. Seta, *Biomaterials*, 2013, **34**, 9220–9226.

14. P. J. Patel, N. S. Acharya, and S. R. Acharya, *Drug delivery*, 2013, **20**, 143–155.

15. S. Mirsadeghi, R. Dinarvand, M. H. Ghahremani, M. R. Hormozi-Nezhad, Z. Mahmoudi, M. J. Hajipour, F. Atyabi, M. Ghavami, and M. Mahmoudi, *Nanoscale*, 2015, **7**, 5004–5013.

16. R. Huang, R. P. Carney, F. Stellacci, and B. L. Lau, *Nanoscale*, 2013, **5**, 6928–6935.

17. C. Cabaleiro-Lago, O. Szczepankiewicz, and S. Linse, *Langmuir*, 2012, **28**, 1852–1857.

18. E. P. O'Brien, J. E. Straub, B. R. Brooks, and D. Thirumalai, *The journal of physical chemistry letters*, 2011, **2**, 1171–1177.

19. K. E. Marshall, K. L. Morris, D. Charlton, N. O'Reilly, L. Lewis, H. Walden, and L. C. Serpell, *Biochemistry-Columbus*, 2011, **50**, 2061.

20. M. J. Roberti, M. Morgan, G. Menéndez, L. I. Pietrasanta, T. M. Jovin, and E. A. Jares-Erijman, *Journal of the American Chemical Society*, 2009, **131**, 8102–8107.

21. J. A. Yang, W. Lin, W. S. Woods, J. M. George, and C. J. Murphy, *The Journal of Physical Chemistry B*, 2014, **118**, 3559–3571.

Nanoscale Accepted Manuscript

22. J. A. Yang, B. J. Johnson, S. Wu, W. S. Woods, J. M. George, and C. J. Murphy, *Langmuir*, 2013.

23. L. Kjaer, L. Giehm, T. Heimburg, and D. Otzen, *Biophysical journal*, 2009, **96**, 2857–2870.

24. Y. D. Álvarez, J. A. Fauerbach, J. V. Pellegrotti, T. M. Jovin, E. A. Jares-Erijman, and F. D. Stefani, *Nano letters*, 2013, **13**, 6156–6163.

25. C. Galvagnion, A. K. Buell, G. Meisl, T. C. Michaels, M. Vendruscolo, T. P. Knowles, and C. M. Dobson, *Nature chemical biology*, 2015.

26. B. Klajnert, T. Wasiak, M. Ionov, M. Fernandez-Villamarin, A. Sousa, J. Correa, R. Riguera, and E. Fernandez-Megia, *Nanomedicine: Nanotechnology, Biology and Medicine*, 2012.

27. K. Langer, S. Balthasar, V. Vogel, N. Dinauer, H. Von Briesen, and D. Schubert, *International Journal of Pharmaceutics*, 2003, **257**, 169–180.

28. V. Mishra, S. Mahor, A. Rawat, P. N. Gupta, P. Dubey, K. Khatri, and S. P. Vyas, *Journal of drug targeting*, 2006, **14**, 45–53.

29. R. H. Christenson, P. Behlmer, J. Howard, J. B. Winfield, and L. M. Silverman, *Clinical chemistry*, 1983, **29**, 1028–1030.

30. H. Kouchakzadeh, S. A. Shojaosadati, F. Tahmasebi, and F. Shokri, *International journal of pharmaceutics*, 2013, **447**, 62–69.

31. H. Mohammad-Beigi, S. A. Shojaosadati, D. Morshedi, A. Arpanaei, and A. T. Marvian, *Journal of Nanoparticle Research*, 2015, **17**, 1–16.

32. N. Lorenzen, L. Lemminger, J. N. Pedersen, S. B. Nielsen, and D. E. Otzen, *FEBS letters*, 2014, **588**, 497–502.

33. J. S. Pedersen, *Journal of applied crystallography*, 2004, **37**, 369–380.

34. Y. Li, R. Beck, T. Huang, M. C. Choi, and M. Divinagracia, *Applied Crystallography*, 2008, **41**, 1134–1139.

35. O. Glatter, *Journal of Applied Crystallography*, 1977, **10**, 415–421.

36. J. S. Pedersen, S. Hansen, and R. Bauer, *European biophysics journal*, 1994, **22**, 379–389.

37. M. Stieger, W. Richtering, J. S. Pedersen, and P. Lindner, *The Journal of chemical physics*, 2004, **120**, 6197–6206.

38. L. Giehm and D. E. Otzen, *Analytical biochemistry*, 2010, **400**, 270–281.

39. A. M. Morris, M. A. Watzky, J. N. Agar, and R. G. Finke, *Biochemistry*, 2008, **47**, 2413–2427.

Nanoscale Accepted Manuscript

40. L. Nesgaard, B. Vad, G. Christiansen, and D. Otzen, *Biochimica et Biophysica Acta (BBA)-Proteins and Proteomics*, 2009, **1794**, 84–93.

41. J. Wang, U. B. Jensen, G. V. Jensen, S. Shipovskov, V. S. Balakrishnan, D. Otzen, J. S. Pedersen, F. Besenbacher, and D. S. Sutherland, *Nano letters*, 2011, **11**, 4985–4991.

42. L. A. Munishkina and A. L. Fink, *Biochimica et Biophysica Acta (BBA)-Biomembranes*, 2007, **1768**, 1862–1885.

43. V. N. Uversky, J. Li, and A. L. Fink, *Journal of Biological Chemistry*, 2001, **276**, 10737–10744.

44. L. Giehm, D. I. Svergun, D. E. Otzen, and B. Vestergaard, *Proceedings of the National Academy of Sciences*, 2011, **108**, 3246–3251.

45. J. Goers, V. N. Uversky, and A. L. Fink, *Protein science*, 2003, **12**, 702–707.

46. A. D. Cardin and H. Weintraub, *Arteriosclerosis, Thrombosis, and Vascular Biology*, 1989, **9**, 21–32.

47. N. Taebnia, D. Morshedi, M. Doostkam, S. Yaghmaei, F. Aliakbari, G. Singh, and A. Arpanaei, *RSC Advances*, 2015, **5**, 60966–60974.

48. N. Lorenzen, S. I. Cohen, S. B. Nielsen, T. W. Herling, G. Christiansen, C. M. Dobson, T. P. Knowles, and D. Otzen, *Biophysical journal*, 2012, **102**, 2167–2175.

49. S. I. Cohen, M. Vendruscolo, M. E. Welland, C. M. Dobson, E. M. Terentjev, and T. P. Knowles, *The Journal of chemical physics*, 2011, **135**, 065105.

50. P. M. Martins, *Prion*, 2013, **7**, 136–139.

51. S. Linse, C. Cabaleiro-Lago, W. F. Xue, I. Lynch, S. Lindman, E. Thulin, S. E. Radford, and K. A. Dawson, *Proceedings of the National Academy of Sciences*, 2007, **104**, 8691–8696.

52. R. Shaw, H. Mantsch, and B. Chowdhry, *Canadian journal of chemistry*, 1993, **71**, 1334–1339.

53. S. Zhang, M. Andreasen, J. T. Nielsen, L. Liu, E. H. Nielsen, J. Song, G. Ji, F. Sun, T. Skrydstrup, F. Besenbacher, and others, *Proceedings of the National Academy of Sciences*, 2013, **110**, 2798–2803.

54. N. Lorenzen, S. B. Nielsen, A. K. Buell, J. D. Kaspersen, P. Arosio, B. S. Vad, W. Paslawski, G. Christiansen, Z. Valnickova-Hansen, M. Andreasen, and others, *Journal of the American Chemical Society*, 2014, **136**, 3859–3868.

Nanoscale Accepted Manuscript

Caption to Tables

Table 1. Main parameters in the structural model for *α*SN adsorption on HSA and PEI-HSA NPs fitted to the SAXS data.

Table 2. Secondary structure content of fibrils formed alone and in the presence of either HSA or PEI-HSA NPs.

Nanoscale Accepted Manuscript

Table 1.

	Radius (nm)	Scale of fluctuation term
HSA NPs	36.2±0.3	1.3±1.2
HSA NPs+*α*SN	36.0±0.2	152±11
PEI-HSA NPs	37.3±0.2	27±9
PEI-HSA NPs+*α*SN	39.2±0.3	132±9

Table 2.

	Wavelength (cm^{-1})		
	1629 (Antip. β-sheet)	**1654 Unordered**	**1673 Turn or β-sheet**
***α*SN fibrils**	61.32±0.8	23.41±0.7	15.27±0.7
+ HSA NPs	60.35±1	24.8±0.9	14.85±0.3
+ PEI-HSA NPs	59.6±0.9	24.9±1	15.5±0.4

Nanoscale Accepted Manuscript

Caption to Figures

Fig. 1. Interaction of αSN with the NPs. (A) Adsorption of αSN onto the surface of NPs. The supernatant was analyzed by UV-visible at 280 nm and the concentration of NPs was 0.5 mg/mL. The continuous lines represent the Langmuir model calculation. (B) Fluorescence anisotropy values of αSN alone and incubated with either HSA or PEI-HSA NPs (mean ± SD, n = 3, *$p < 0.05$ significant compared with αSN). (C) SAXS data (scattering intensity I (q) vs length of scattering vector (q) for free αSN, HSA NPs, PEI-HSA NPs, HSA NPs+ αSN, and PEI-HSA NPs+ αSN. The lines are the best fit to the data of the models described in the text. Inset shows the SAXS data of αSN. Far-UV CD spectra of αSN alone and incubated with (D) HSA NPs, (E) PEI-HSA NPs, and (F) PEI.

Fig. 2. The effect of the NPs on αSN fibrillation. Effect of (A) HSA NPs and (B) PEI-HSA NPs at different concentrations on αSN fibrillation monitored by ThT fluorescence. The continuous lines represent fits to eq. 1, and the arrow indicates the increasing concentration of the NPs. Kinetic parameters for αSN fibrillation as a function of various concentrations of HSA and PEI-HSA NPs relative to the values in the absence of the NPs ((C) relative growth rate ($v/v_{control}$), (D) relative half time ($t_{1/2}/t_{1/2,control}$), and (E) relative lag time ($t_N/t_{N,control}$)).

Fig. 3. Schematic illustration of the possible mechanism of the effect of HSA and PEI-HSA NPs on the αSN's adsorption, orientation and aggregation. Weak interactions with HSA NPs have no effect on αSN conformation and fibrillation, while strong interactions with PEI-HSA NPs alter αSN conformation and accelerate the primary nucleation step of aggregation.

Fig. 4. Kinetic analysis of the effect of the NPs on the fibrillation of αSN at different NaCl concentrations (50-300 mM). Effect of (A) HSA NPs (50 μg/mL) and (B) PEI-HSA NPs (50 μg/mL) at different NaCl concentrations on αSN fibrillation monitored by ThT fluorescence. Kinetic parameters ((C) growth rate (v), (D) half time ($t_{1/2}$), and (E) lag time (t_N)) and normalized maximum fluorescence intensity (F) of αSN fibrillation in the presence and absence of HSA NPs and PEI-HSA NPs as a function of various NaCl concentrations.

Nanoscale Accepted Manuscript

Fig. 5. (A) Electron microscopy of αSN incubated alone andin the presence of either HSA or PEI-HSA NPs after 1, 4 and 24 h (at 150 mM salt concentration). Scale bar, 200 nm. (B) AFM images of the αSN fibril morphology formed after 24 h incubation of αSN alone (B1) and in the presence of either HSA (B2) or PEI-HSA NPs (B3) (at 150 mM salt concentration). Scale bar, 500 nm. (C) AFM images of a twisted αSN fibril. (D) Height profile along the major twisted fibril running from top to bottom in image C showing clear height periodicity. (E) Cross sectional profiles of the fibril in C. (F) AFM morphology image of aggregates of αSN formed in the presence of PEI-HSA NPs. (G) AFM images of PEI-HSA NPs.

Fig. 6. The effect of the NPs on the SEC profiles of the supernatant of αSN samples. All spectra are averages of duplicates. Percentage value of oligomers formed in the presence andabsence of the NPs are listed in the table.

Fig. 7. Calcein release from DOPG vesicles induced by (A) HSA NPs, (B) PEI-HSA NPs, (C) oligomers + HSA NPs, and (D) oligomers + PEI-HSA NPs. The arrows indicate the direction of increased NPs concentration.

Fig. 8. Viability of PC-12 cells after 24 h incubation with αSN aggregates formed alone and in the presence of either HSA (50 μg/mL) or PEI-HSA NPs (25 μg/mL and 50 μg/mL)over different times (0-24 h).

Nanoscale Accepted Manuscript

Fig. 1.

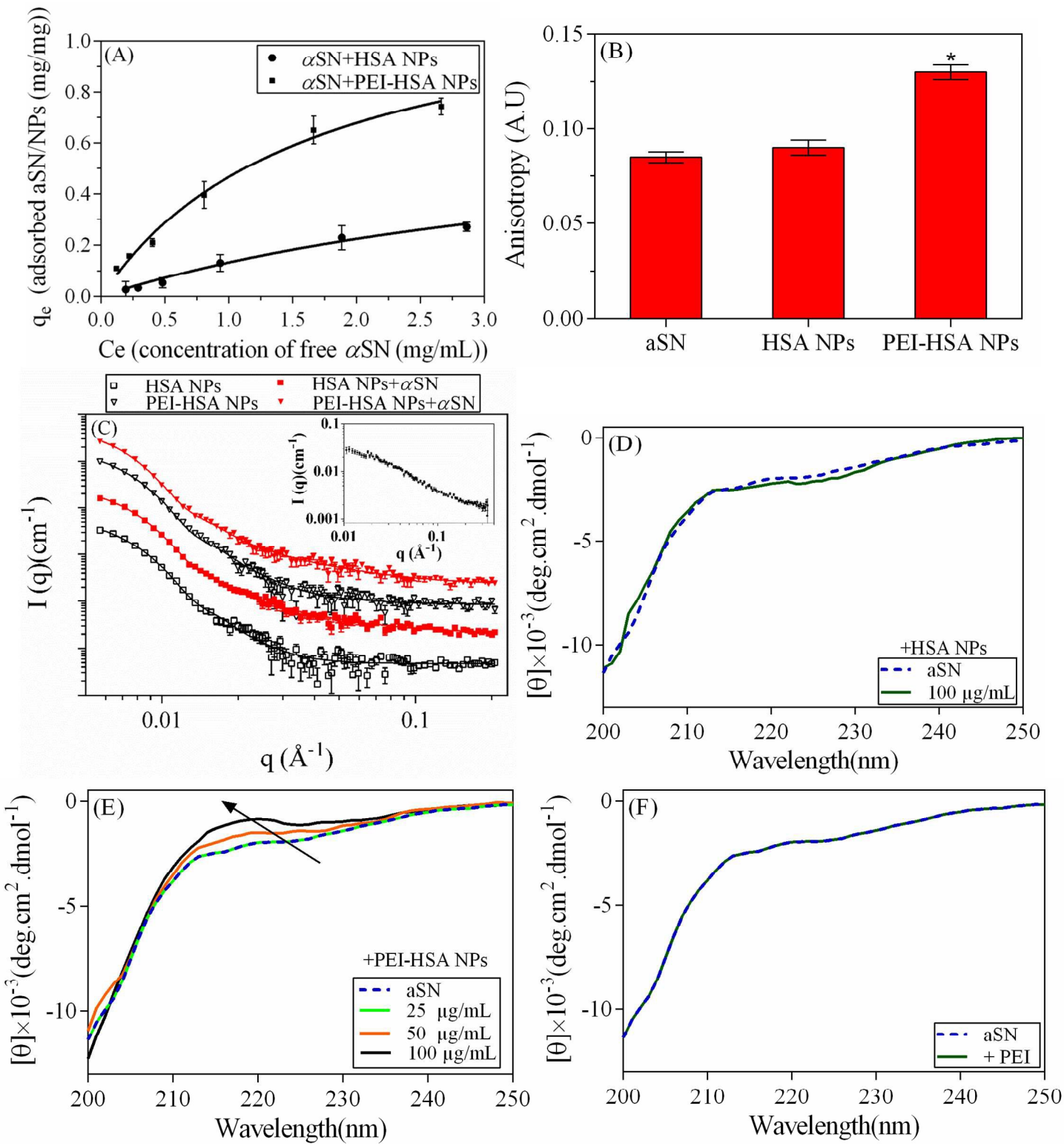

Nanoscale Accepted Manuscript

Fig. 2.

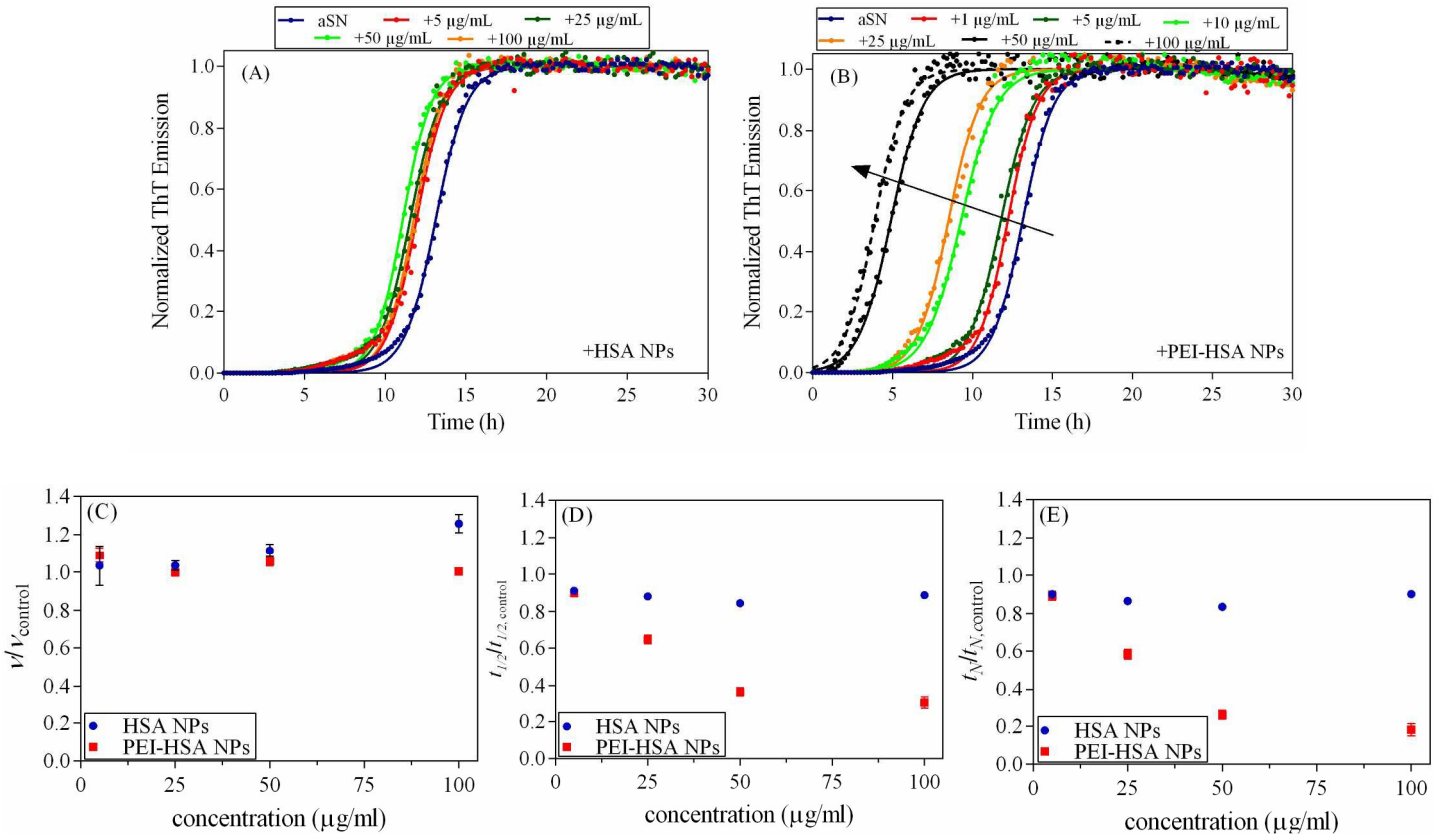

Nanoscale Accepted Manuscript

Fig. 3.

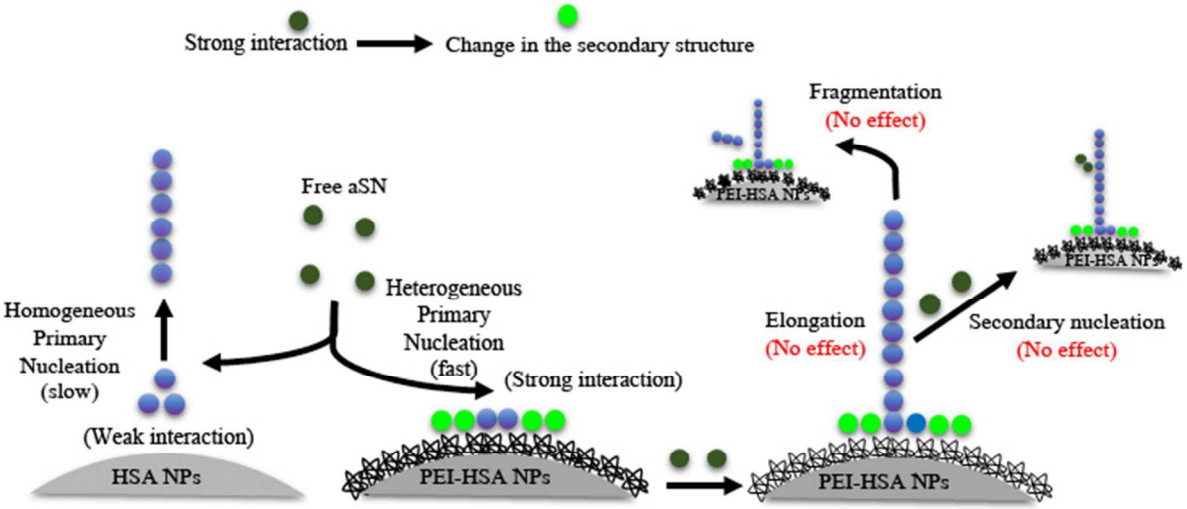

Nanoscale Accepted Manuscript

Fig. 4.

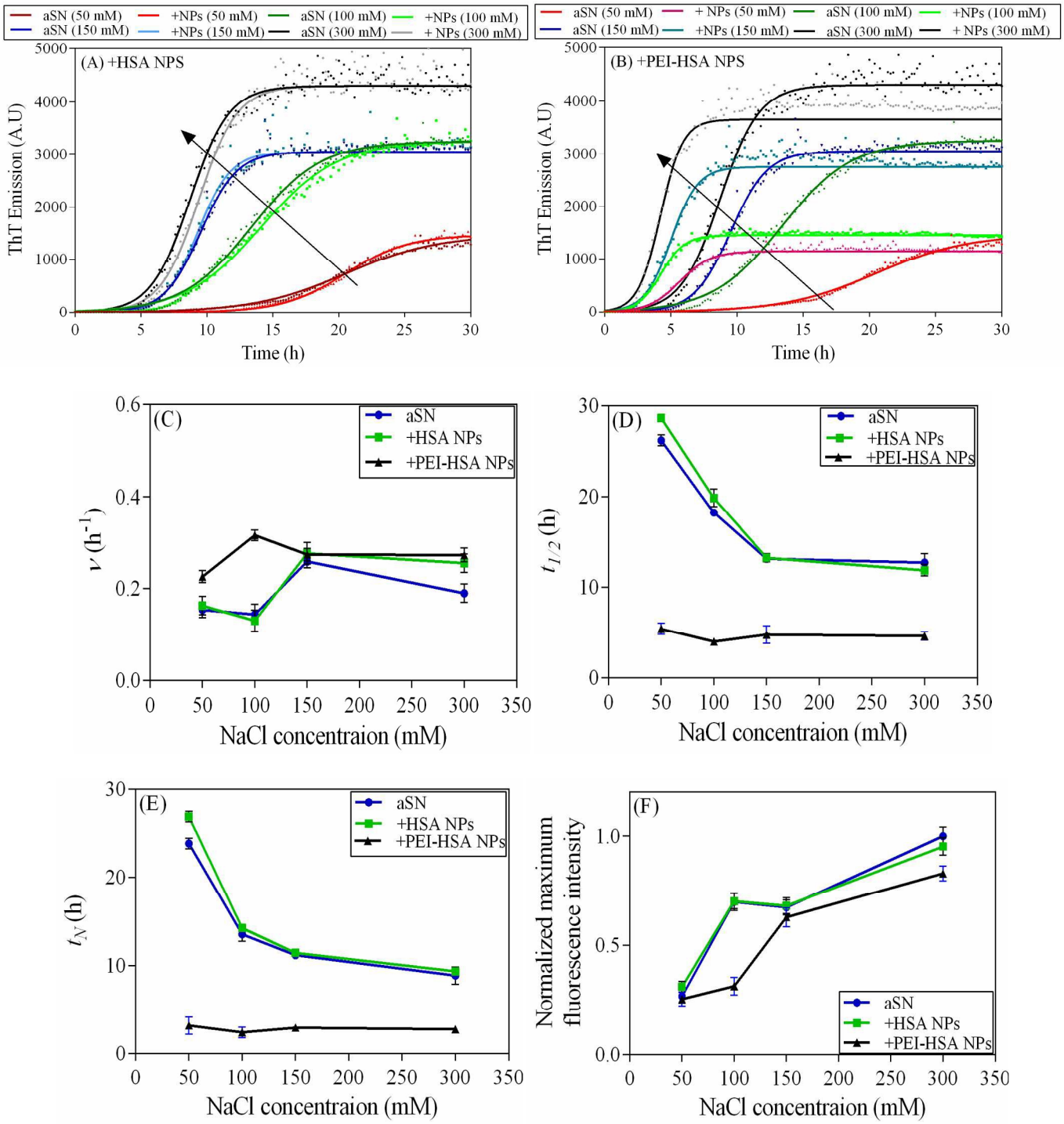

Nanoscale Accepted Manuscript

Fig. 5.

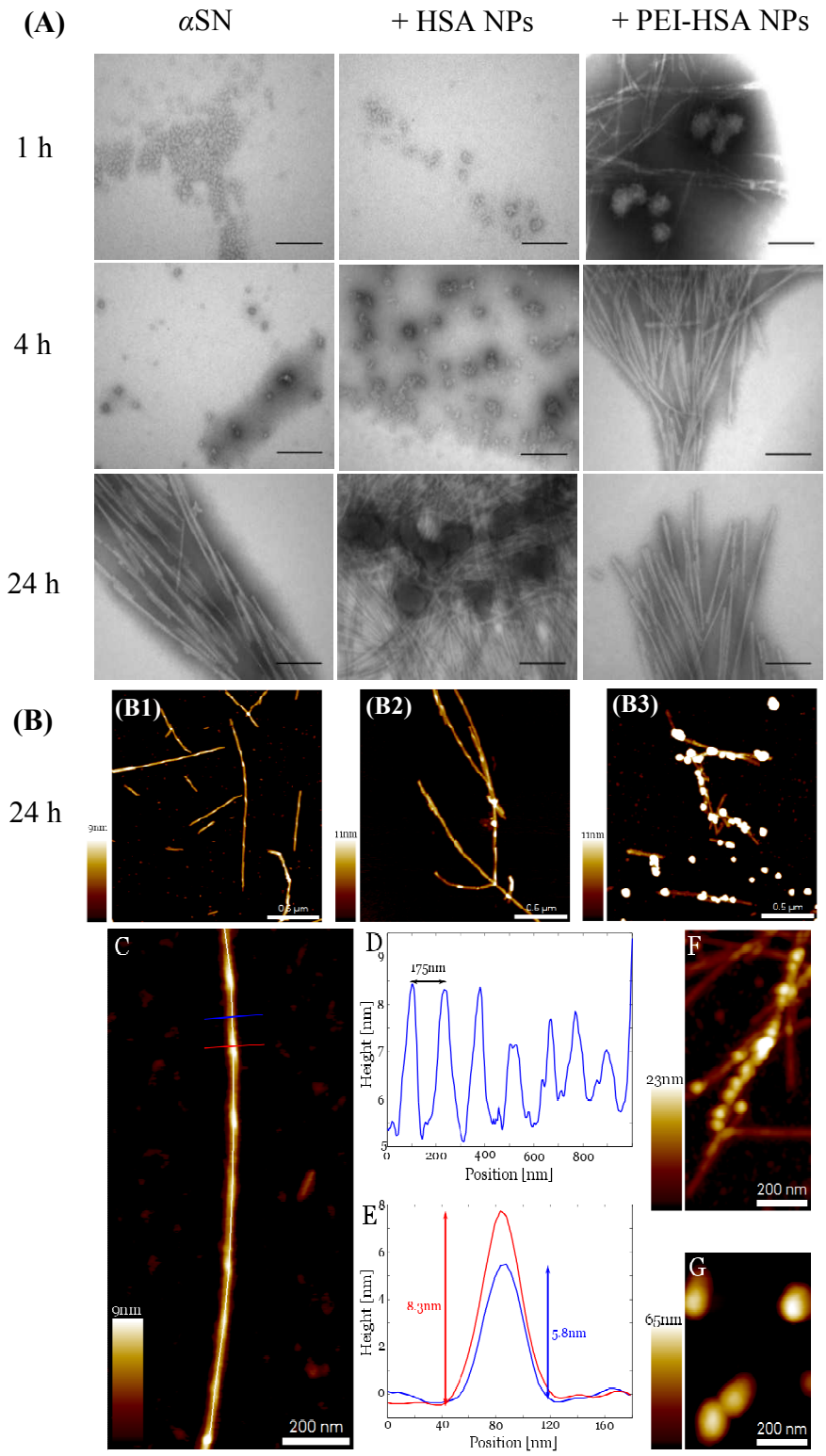

Nanoscale Accepted Manuscript

Fig. 6.

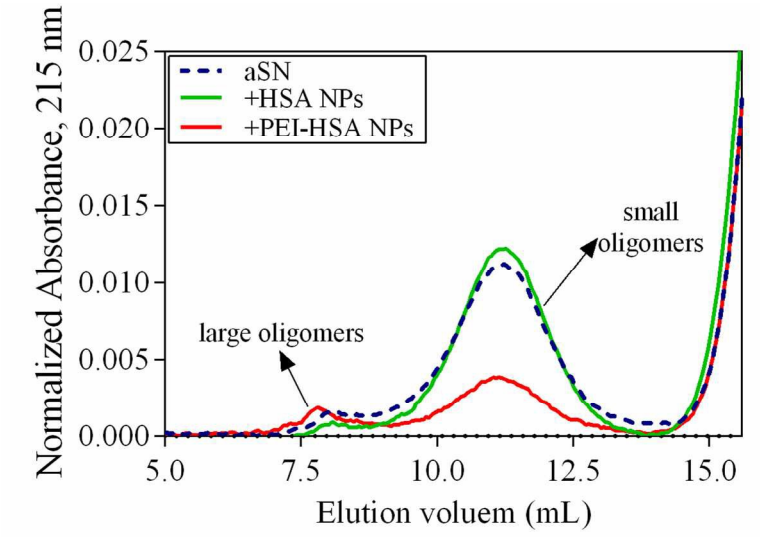

	Small oligomers (%)
αSN	1.13±0.07 *
+PEI-HSA NPs	0.37±0.02 *
+HSA NPs	1.20±0.045

Nanoscale Accepted Manuscript

Fig. 7.

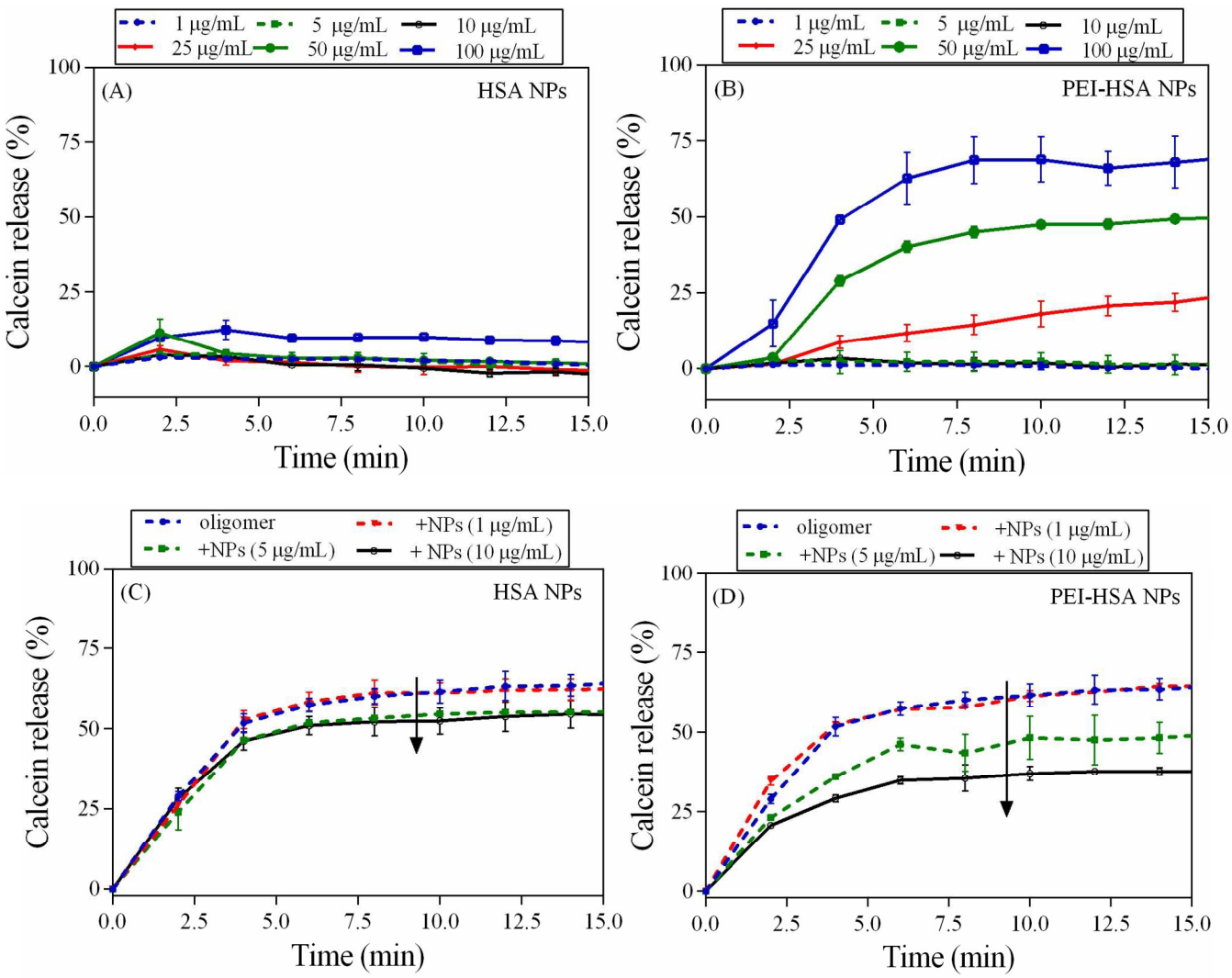

Nanoscale Accepted Manuscript

Fig. 8.

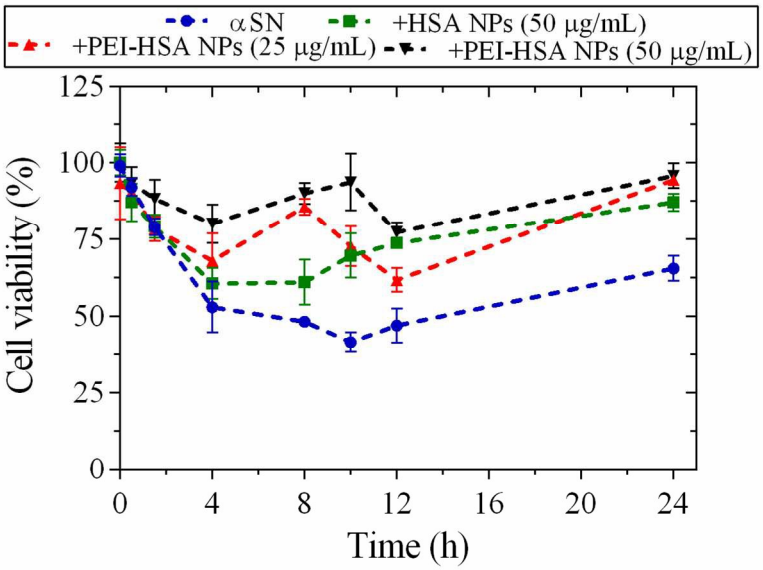

Nanoscale Accepted Manuscript